The Journal of Chemical Physics

Surface hopping with a manifold of electronic states. I. Incorporating surface-leaking to capture lifetimes

Cite as: J. Chem. Phys. **142**, 084109 (2015); https://doi.org/10.1063/1.4908032
Submitted: 05 December 2014 • Accepted: 01 February 2015 • Published Online: 25 February 2015

Wenjun Ouyang, Wenjie Dou and Joseph E. Subotnik

Surface hopping with a manifold of electronic states. I. Incorporating surface-leaking to capture lifetimes

Wenjun Ouyang, Wenjie Dou, and Joseph E. Subotnik[a)]
Department of Chemistry, University of Pennsylvania, Philadelphia, Pennsylvania 19104, USA

(Received 5 December 2014; accepted 1 February 2015; published online 25 February 2015)

We investigate the incorporation of the surface-leaking (SL) algorithm into Tully's fewest-switches surface hopping (FSSH) algorithm to simulate some electronic relaxation induced by an electronic bath in conjunction with some electronic transitions between discrete states. The resulting SL-FSSH algorithm is benchmarked against exact quantum scattering calculations for three one-dimensional model problems. The results show excellent agreement between SL-FSSH and exact quantum dynamics in the wide band limit, suggesting the potential for a SL-FSSH algorithm. Discrepancies and failures are investigated in detail to understand the factors that will limit the reliability of SL-FSSH, especially the wide band approximation. Considering the easiness of implementation and the low computational cost, we expect this method to be useful in studying processes involving both a continuum of electronic states (where electronic dynamics are probabilistic) and processes involving only a few electronic states (where non-adiabatic processes cannot ignore short-time coherence). © *2015 AIP Publishing LLC.* [http://dx.doi.org/10.1063/1.4908032]

I. INTRODUCTION

Electronic dynamics usually come in two flavors. First, some electron relaxation events do not involve much coherence and can best be described probabilistically. In such cases, electrons are ejected into a continuum. Examples of such processes include chemi-ionization[1–6] and Auger recombination. Among chemi-ionization processes, Penning ionization has attracted much attention because of the large cross section in collisional reactions involving metastable atoms and molecules. As a result Penning ionization is a significant process in characterizing thermal plasma, electrical discharges, and the production of laser system, as well as in atmospheric chemistry.[6] For Auger recombination, Interatomic Coulombic Decay (ICD) is a hot topic nowadays in the literature because the process can be highly efficient when the excited ion has many neighbors and ICD leads to many examples of fragmentation.[7–11] The simplest approach for modeling these processes is to use straightforward classical probability theory.[1,2,12]

While the processes above have a bath of electronic states which leads to a certain amount of electronic friction and a lack of coherence, a second class of non-adiabatic processes involves only a minimal number of electronic states. These non-adiabatic problems in chemistry include most forms of photoexcited dynamics at low energies in solution, including electron transfer and electronic energy transfer,[13–20] spin relaxation,[21–24] intersystem-crossing,[25–29] etc. These coherent dynamics are important for understanding organic enzymes, molecular photocatalysis, and organic photoexcitations. In practice, modeling this second class of relaxation events requires different tools from the first class. Nuclei must move coherently for a reasonably long period of time. In practice, a few methods exist for modeling such dynamics including Meyer-Miller-Stock-Thoss (MMST)/Poisson bracket mapping equation (PBME),[30–38] multiple spawning,[39–41] and fewest-switches surface hopping (FSSH).[42] Given our group's recent experience with FSSH, we will focus on FSSH.

Now, many processes in nature involve both short time electronic coherent and long time incoherent probabilistic electronic dynamics. However, even though both areas have been studied extensively for a long time both experimentally and theoretically, there are few efficient theoretical approaches to address both problems above where competition between coherent non-adiabatic processes and incoherent relaxation processes becomes predominate and interesting. The goal of the present article is to study a surface-leaking FSSH (SL-FSSH) algorithm that combines Preston's surface-leaking[1] with Tully's FSSH algorithm,[42] benchmark the performance of SL-FSSH in system-bath model problems against quantum scattering calculation, and investigate dynamics beyond the wide band approximation to characterize the limitations of our algorithm. In Paper II, we will discuss and benchmark a very similar surface hopping approach in the context of a many body physics problem (the Anderson-Holstein model).[43]

An outline of this article is as follows. In Sec. II, we review briefly Tully's FSSH algorithm and Preston's surface-leaking (SL) algorithm, and then outline the SL-FSSH algorithm. In Sec. III, we compare exact and SL-FSSH results for three model problems with different sets of parameters. In Sec. IV, we investigate the sources of error in the SL-FSSH calculation, and we discuss the wide band approximation and its breakdown. Section V concludes this paper.

II. SURFACE-LEAKING FSSH

A. Tully's fewest-switches surface hopping

For modeling photoexcited molecular dynamics in solution, the most common prescription is Tully's FSSH algorithm.[42] A representative Hamiltonian in a diabatic basis can

a)Electronic mail: subotnik@sas.upenn.edu

be written as

$$\mathbf{H} = \mathbf{T}_n + \mathbf{H}_e, \tag{1}$$

where $\mathbf{T}_n$ is the nuclear kinetic energy operator, and the electronic Hamiltonian $\mathbf{H}_e$ can be written as

$$\mathbf{H}_e = \sum_i E_i(\mathbf{R}) \left|\Xi_i\right\rangle \left\langle\Xi_i\right| + \sum_{i\neq j} \mathcal{V}_{ij}(\mathbf{R}) \times \left(\left|\Xi_i\right\rangle \left\langle\Xi_j\right| + \left|\Xi_j\right\rangle \left\langle\Xi_i\right|\right), \tag{2}$$

where $|\Xi_i\rangle$ is the ith electronic diabat, E_i is the energy of diabatic state i, and $\mathcal{V}_{ij}$ is the diabatic coupling between states i and j. The premise of FSSH is that electrons are treated quantum mechanically while nuclei are classical, while all calculations are performed exclusively in an adiabatic basis

$$\mathbf{H}_e = \sum_j V_{jj} \left|\Phi_j\right\rangle \left\langle\Phi_j\right|, \tag{3}$$

where V_{jj} is the adiabatic energy of state j and $\left|\Phi_j\right\rangle$ is the corresponding adiabat. In detail, while the electrons move in the instantaneous electric field caused by the nuclei, the nuclei move along one single potential energy surface (PES) at a time and hop (once in a while) between different PESs to account for electronic relaxation. Preston and Tully first suggested that hops should be made *post-facto*,[44] whereby one can decide if he/she has gone through a crossing. According to Tully's later FSSH model,[42] there is a continuous hopping probability at every time step—which depends on both the derivative coupling between adiabatic electronic states and the history of each trajectory. In particular, according to the FSSH algorithm, for each trajectory we must propagate the positions ($\mathbf{R}$) and momenta ($\mathbf{P}$) of each nuclear degree of freedom according to Newton's equations, and the corresponding electronic quantum amplitudes (c_i) for each adiabatic electronic state i according to time-dependent Schrödinger equation. The hopping can then be extracted from the evolution of this trajectory.

While the FSSH algorithm has several known problems modeling photoexcited systems with a few electronic states (including decoherence[45–64]), another obstacle posed by the FSSH algorithm is its insistence on an adiabatic basis and the difficulty running FSSH dynamics for systems with large numbers of degrees of freedom. In such a limit, one problem is that the cost of the algorithm increases at least quadratically with the number of electronic states (n_{tot})[65] because one is forced to compute the derivative couplings between all n_{tot} electronic states to propagate the Schrödinger equation. In the limit of a molecular system near a metal surface, the number of electronically adiabatic states becomes very large and standard FSSH becomes impossible. Another practical problem for FSSH is the conundrum of "trivial crossings,"[18] where two or more noninteracting states cross, leading to a spiky derivative coupling in time domain and severely limiting the simulation time step. There has been a lot of recent research[18,66–68] seeking to address this problem. In recent years, Tretiak[18] has studied energy transfer in extended organic chromophores by applying FSSH to simulation with a large manifold of electronic states. For such simulations, he has consistently found that the "trivial crossing" problem cannot be ignored in practice.

To our knowledge, there have been only a few attempts to heuristically amend FSSH dynamics to include manifold of many electronic states (without using brute force). Li *et al.* have proposed a scheme for mixing FSSH dynamics on the ground states with mean-field Ehrenfest dynamics to treat a manifold of excited states.[69] In a set of very interesting papers, Shenvi, Roy, and Tully[70–72] proposed an "Independent Electron Surface Hopping (IESH)" algorithm that has been used to model NO scattering off of a gold surface. For IESH, the basic premise is to discretize a continuum of electronic levels and then run independent trajectories, for which every electron is independent and single excitations of the metal manifold are allowed. Electronic friction is simulated by averaging over the ensemble of trajectories, and Shenvi *et al.* have shown that this model captures vibrational relaxation of the NO molecule as induced by electron transfer to and from the metal. Given the power of the IESH model, we would like to find a very simple extension of FSSH for the case of many electronic states that does not require continuum discretization and that has the smallest possible computational overhead.

B. Surface-leaking algorithm

In contrast to the FSSH algorithm, which is usually applied for only a handful of electronic excited states, there is a different (far less well known, but also far simpler) approach in the literature for treating coupled nuclear-electronic systems with many electronic states. As originally constructed to model the effects of chemi-ionization on atom-diatom collisions,[1] the Preston-Cohen "SL" model was used to predict rearrangement, association, and dissociation branching ratios from atom-diatom collisions.

Conceptually, the surface leaking model is very simple. Consider a Hamiltonian of the form

$$\mathbf{H} = \mathbf{T}_n + \mathbf{H}_s + \mathbf{H}_b + \mathbf{H}_{sb}. \tag{4}$$

Here, $\mathbf{T}_n$ denotes the nuclear kinetic energy operator and $\mathbf{H}_s$ represents the electronic Hamiltonian of the system,

$$\mathbf{H}_s = \sum_j E_j(\mathbf{R}) \left|\Xi_j\right\rangle \left\langle\Xi_j\right|, \tag{5}$$

and $\mathbf{H}_b$ represents a bath of electronic states

$$\mathbf{H}_b = \sum_k \varepsilon_k(\mathbf{R}) \left|k\right\rangle \left\langle k\right|. \tag{6}$$

$\mathbf{H}_{sb}$ signifies the coupling between system and bath which we assume is bilinear in the electronic degrees of freedom and a function of only nuclear position

$$\mathbf{H}_{sb} = \sum_{jk} U_{jk}(\mathbf{R}) \left(\left|\Xi_j\right\rangle \left\langle k\right| + \left|k\right\rangle \left\langle\Xi_j\right|\right). \tag{7}$$

For an infinite bath, the system-bath interaction is quantified by its hybridization function

$$\Gamma_j(\mathbf{R}) = 2\pi\rho(E_j(\mathbf{R}))\overline{\left|U_{jk}(\mathbf{R})\right|^2}. \tag{8}$$

Here, $\left|U_{jk}\right|^2$ is averaged over all states $|k\rangle$ with energy $E_j(\mathbf{R})$. If $\left|U_{jk}\right|^2$ is truly independent of k, $\Gamma_j(\mathbf{R})/\hbar$ can be thought of as the lifetime of the system electronic state j (when the nuclei are at position $\mathbf{R}$). The basic premise of the surface leaking algorithm is to run nuclear dynamics along a potential

energy surface of the system, while damping the population of the system by $\Gamma_j(\mathbf{R})\Delta t/\hbar$ at every time step (where Δt is the simulation time step).

C. SL-FSSH

Given how many modern experiments involve photoexcited systems of molecule-metal interface,[73–75] it would seem very natural to merge the surface leaking and surface hopping algorithms. In so doing, one would like to include both the short-time electronic coherence present in the FSSH algorithm (so as to capture potential energy surface crossings) with the long time irreversible electronic relaxation present in the SL algorithm (so as to capture electronic dissipation into a metallic bath). In other words, we would like to replace the simple system Hamiltonian in Eq. (5) with the more complex Hamiltonian in Eq. (2).

In principle, merging SL and FSSH should be straightforward to achieve. On the one hand, one ought to diagonalize the electronic states of the system and run FSSH dynamics along such adiabatic states; on the other hand, one does not want to include bath states in the above diagonalization, and one would prefer to use perturbation theory on the system-bath coupling to model the population leakage from the system to the bath. In theory, this approach should be equivalent to including complex energies in the time-dependent electronic Schrödinger equation[76] to damp out population and then allow the FSSH algorithm to dictate naturally how population evolves. In this paper, we want to formalize exactly how the algorithm is applied, discuss the competition between surface leaking and surface hopping, and then formally benchmark the resulting algorithm against exact scattering calculations.

With this in mind, a step-by-step description of our SL-FSSH algorithm is as follows:

1. Initialize all FSSH variables—the positions $\mathbf{R}$ and momenta $\mathbf{P}$ of the nuclei, the current electronic state (active PES) λ, and the electronic amplitudes c_i according to the initial condition. Each trajectory also carries a weight, $N_{sys} = 1$, to represent the population of system.
2. (Same as FSSH) Propagate the nuclei and electronic wave functions for one time step. The nuclei are propagated by classical mechanical equations:

$$\frac{dR^\alpha}{dt} = \frac{P^\alpha}{M^\alpha}, \tag{9}$$

$$\frac{dP^\alpha}{dt} = -\nabla_\alpha V_{\lambda\lambda}(\mathbf{R}), \tag{10}$$

where α labels a classical degree of freedom, $V_{ij}(\mathbf{R})$ are the matrix elements of electronic Hamiltonian at position $\mathbf{R}$ in an adiabatic basis, and M is the mass of a nucleus. The electronic amplitudes are propagated by time-dependent Schrödinger equation

$$i\hbar\frac{dc_k}{dt} = \sum_j c_j\left(V_{kj}(\mathbf{R}) - i\hbar\frac{d\mathbf{R}}{dt}\cdot\mathbf{d}_{kj}(\mathbf{R})\right), \tag{11}$$

where $\mathbf{d}_{kj}(\mathbf{R})$ is the non-adiabatic coupling vector between state k and j at position $\mathbf{R}$.

3. (Same as FSSH) Hopping probabilities $g_{\lambda j}$ from the current electronic state λ to all other states j are determined as in FSSH

$$g_{\lambda j} = -\frac{2}{|c_\lambda|^2}\mathrm{Re}\left(c_\lambda c_j^*\mathbf{d}_{j\lambda}(\mathbf{R})\cdot\frac{d\mathbf{R}}{dt}\right). \tag{12}$$

A uniform random number ξ in $[0,1]$ is then generated and compared with the cumulative hopping probability to determine the target state. For instance, if $\lambda = 1$ and $\xi < g_{12}$ then current electronic state changes to state 2; if $g_{12} \le \xi < g_{12} + g_{13}$, the current electronic state changes to state 3, etc. If ξ is larger than the sum $\sum_j g_{\lambda j}$, then no hopping happens and current electronic state remains unchanged.
4. (Same as FSSH) If a hop does not occur, proceed to step 5. If there is a hop, the momentum must be rescaled to account for energy conservation. The momentum is rescaled in the direction of the non-adiabatic coupling vector (assuming we are hopping from current state λ to state j):

$$\mathbf{P}^{new} = \mathbf{P} + \Delta P\hat{\mathbf{d}}_{\lambda j}(\mathbf{R}), \tag{13}$$

$$\sum_\alpha\frac{(P^{\alpha,new})^2}{2M^\alpha} + V_{jj}(\mathbf{R}) = \sum_\alpha\frac{(P^\alpha)^2}{2M^\alpha} + V_{\lambda\lambda}(\mathbf{R}), \tag{14}$$

where $\hat{\mathbf{d}}_{\lambda j}(\mathbf{R})$ is the unit vector of non-adiabatic coupling vector at position $\mathbf{R}$. If $\mathbf{P}^{new}$ is complex, the hop is not allowed. If $\mathbf{P}^{new}$ is real, a hop is allowed and the active surface is changed (in this case, to j).
5. (From SL) For a general Hamiltonian, the electronic bath might couple to an arbitrary electronic state of the system—which might be an adiabatic or diabatic state (or some other entirely different state). Assuming that the bath is coupled to a diabatic system state, we calculate the diabatic population $n_i^{(diab)}$ on each state i; for now, this is done using only the active surface (which is labeled to Method #1 in Ref. 77; see below for a few details). Then, we calculate the probability $L_i(\mathbf{R})$ of leaking out of the system from state i to its corresponding bath (the same as in the SL algorithm):

$$L_i(\mathbf{R}) = \frac{\Gamma_i(\mathbf{R})\Delta t}{\hbar}. \tag{15}$$

Finally, the new and reduced population remaining on system state is updated

$$N_{sys}^{(new)} = N_{sys}^{(old)}\left(1 - \sum_i n_i^{(diab)}L_i(\mathbf{R})\right). \tag{16}$$

Return to step 2.

At the end of the calculation, all trajectories must be summed and weighted with N_{sys}, which must be in the range $[0,1]$. Because N_{sys} does not have any feedback into the FSSH dynamics, SL-FSSH is very easy and straightforward to implement. Note here that, by ignoring the hopping from the bath back to the system, we are assuming that the bath is infinitely wide. In Sec. IV C, we will discuss the use of SL-FSSH beyond the wide band approximation.

One word is now in order about how to calculate diabatic populations assuming that the bath is coupled to the diabatic populations. In this case, Ref. 77 shows that there are three straightforward means to extract diabatic populations: one can use either (i) the active electronic surface, (ii) the electron

amplitudes c_i, or (iii) a combination of both active surface and amplitudes. While the third option is the most rigorous,[77] unfortunately, such an option also requires that all trajectories be coupled to each other in real time, and thus is not practical for large systems. At the same time, option (ii) simply cannot recover correct long time populations.[77] Thus, option (i) is likely the only possible balance between accuracy and scalability.

III. RESULTS

To investigate the algorithm presented above, we will study a set of system-bath interaction models, all restricted to one nuclear degree of freedom. The electronic system is one or two discrete states, and the bath in principle represents a continuum of states. In practice, the bath is discretized into a set of 501 parallel states for the exact scattering calculations (see Appendix for the algorithm). The coupling between system and bath is position dependent and there is no intra-bath interaction. All simulations begin with one system state populated, followed subsequently by a combination of interstate transfer and/or relaxation into the bath. For our scattering calculation, we examine transmission and reflection probabilities. We will investigate two extreme cases: (i) a primary system state crosses a bath of parallel electronic states; (ii) a primary system state is parallel to a set of bath states. See Fig. 1 for the diabatic PESs for the three model problems we will study.

A. Model #1: One system state couples to a set of nonparallel bath states

Model #1 is the simplest Hamiltonian we consider. This model can be treated easily with the surface-leaking algorithm alone (without invoking FSSH). There is only one system state

$$V_{sys}(x) = A\tanh(Bx), \tag{17}$$

where $A = 0.01$ a.u. and $B = 1.6$ a.u. The set of bath states take the following form:

$$V_{bath}(x) = -V_{sys}(x) + \Delta, \tag{18}$$

where Δ is a shift in energy (which can be either positive or negative). A set of diabatic PES are shown in Fig. 1(a) for five different energy offsets, $\Delta = 0.008, 0.004, 0, -0.004, -0.008$, all in atomic unit.

The diabatic coupling between system and bath is given by V_{sb}:

$$V_{sb}(x) = C\exp(-Dx^2), \tag{19}$$

where $D = 1.0$ a.u. To make the definition of C consistent with an infinite set of bath states, C is defined as

$$C \equiv \sqrt{\frac{\Gamma(0)}{2\pi\rho}} \tag{20}$$

in agreement with Eq. (8). Thus, $\Gamma(0)$ is our free parameter of choice (not C). For our exact scattering calculation where the bath is discretized, the density of states of bath ρ is simply

$$\rho = \frac{N_{bath}}{\Delta E_{bath}}. \tag{21}$$

Here, N_{bath} is the number of states in bath and ΔE_{bath} is the energy range of the bath.

The model problem above is particularly simple because we have only one system state. As such, there are no coherent processes and every trajectory with the same incoming energy gives exactly the same result. In other words, Model #1 can be considered deterministic, so that one trajectory result is sufficient. At the beginning of the SL simulation, we set $n_i^{(diab)}(x)$ in Eq. (16) to be 1 for all x. Let us now explore the transmission and reflection probabilities, first for the bath states and then for the system state.

1. Dynamics of the bath

To explore the distribution of population on the bath states, we run a set of surface-leaking calculations whereby each trajectory is initialized with an incoming particle on left moving along the system state. We consider two different cases with different incoming kinetic energies: (i) the incoming velocity is large enough to transmit along the system state; (ii) the incoming energy is small enough that there will be reflection along

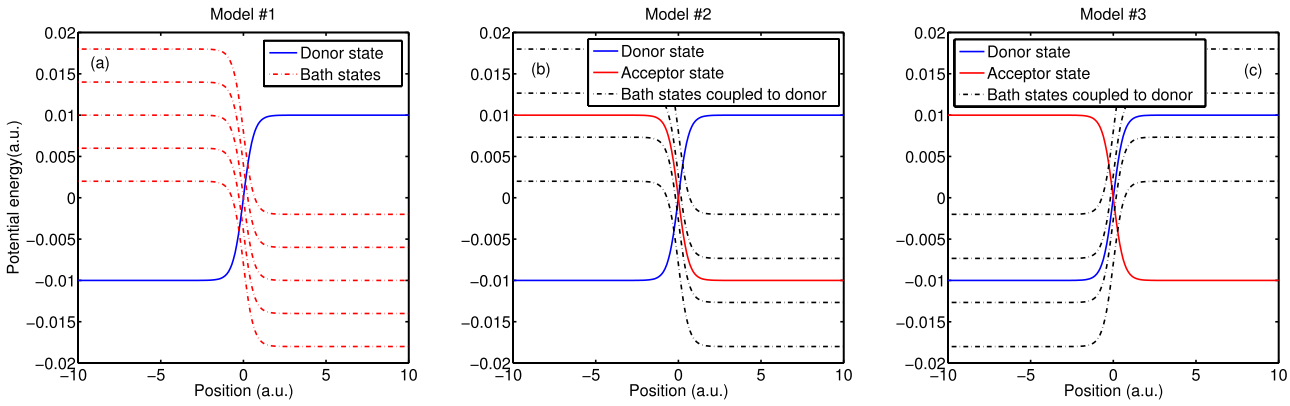

FIG. 1. Three model problems mentioned in this manuscript. The diabatic coupling is not shown. The solid curves are the system states and dash curves are the bath states (of variable width). Note that, as drawn, the Hamiltonians appear to have only 4-5 bath states. In truth, more than 500 bath states were use for the quantum scattering calculations; for the SL-FSSH calculation, the bath is a truly infinite continuum of states. (a) Model #1: one donor state coupled to a nonparallel set of bath states. (b) Model #2: one donor state coupled to one acceptor state while the donor state is coupled to a set of nonparallel bath states. (c) Model #3: one donor state coupled to one acceptor state while the donor state is coupled to a set of parallel bath states.

the system diabat, with the possibility for multiple crossing. To explore the problem in the fully classical limit, we set the nuclear mass to be 100 000 a.u. We set $\Gamma(0) = 10^{-4}$ a.u. to ensure that we are in the weak coupling regime.

In Fig. 2, we plot the transmission probability density for the different bath states as a function of outgoing kinetic energy, according to both exact dynamics and the surface-leaking algorithm.[78] These distributions are obtained by calculating how much population is leaked by each trajectory into the bath at every time step, visualizing the bath state that crosses the system state instantaneously, and then recording the asymptotic potential energy of that crossing bath state. By conservation of energy, we can make a histogram of the distribution of outgoing kinetic energies. For Fig. 2, the incoming kinetic energy is large, 0.025 a.u., so there need not be any reflection. In fact, we find no reflection, so we plot only transmission. Note that larger outgoing kinetic energies correspond to transmission through lower energy channels.

According to Fig. 2, there is a strong overall agreement between surface-leaking and exact results. All SL errors lie on the edges of the kinetic energy distribution. Our strong feeling is that these errors must be caused by nuclear quantum effects, e.g., tunneling. In Sec. IV B, we will redraw Fig. 2 for a particle of smaller mass to reinforce this hypothesis.

In Figs. 3 and 4, we treat a slightly more difficult case. For this calculation, the incoming kinetic energy is 0.015 a.u. In this case, the nucleus has too little energy to transmit forward along the system state, and there will be population reflecting backwards. In Fig. 3, we plot transmission; in Fig. 4, we plot reflection. According to Fig. 4, the SL probability of reflection is in good agreement with exact quantum dynamics; however, there are clear discrepancies in transmission between SL and exact quantum dynamics. On the one hand, according to exact dynamics, we observe oscillations in probability between 0.005 and 0.2 a.u. of kinetic energy. On the other hand, SL predicts a sudden drop in transmission as the outgoing kinetic energy grows and passes 0.02 a.u. At the same time, the exact dynamics predict a smooth peak in population at outgoing energy ~0.006 a.u., while SL predicts a sharp peak in population at the smallest outgoing kinetic energy allowed (0.005 a.u.). These differences will be explored in detail in Sec. IV A but, for now, we comment that these differences should not limit

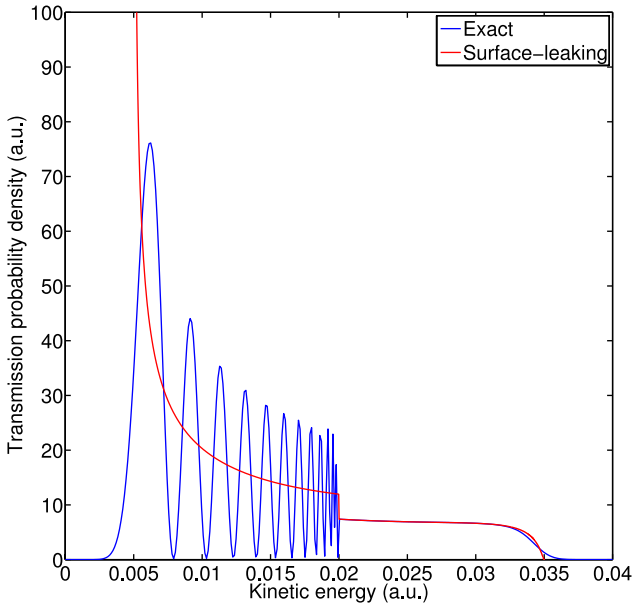

FIG. 3. Model #1: Transmission probability density for the bath states as a function of outgoing kinetic energy according to both exact dynamics and the surface-leaking algorithm. The incoming kinetic energy is 0.015 a.u., the nuclear mass is 100 000 a.u., and $\Gamma(0)$ is 10^{-4} a.u. The differences between exact dynamics and SL will be explored in Sec. IV B.

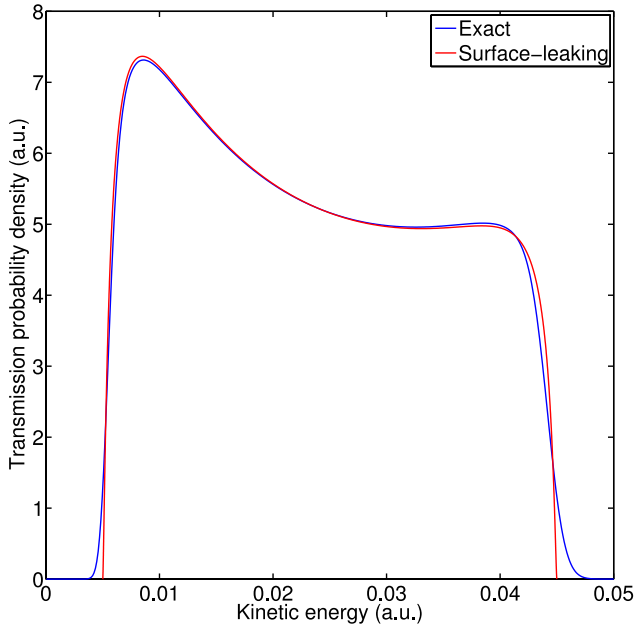

FIG. 2. Model #1: Transmission probability density for the bath states as a function of outgoing kinetic energy according to both exact dynamics and the surface-leaking algorithm. The incoming kinetic energy is 0.025 a.u., the nuclear mass is 100 000 a.u., and $\Gamma(0)$ is 10^{-4} a.u. Note the good agreement.

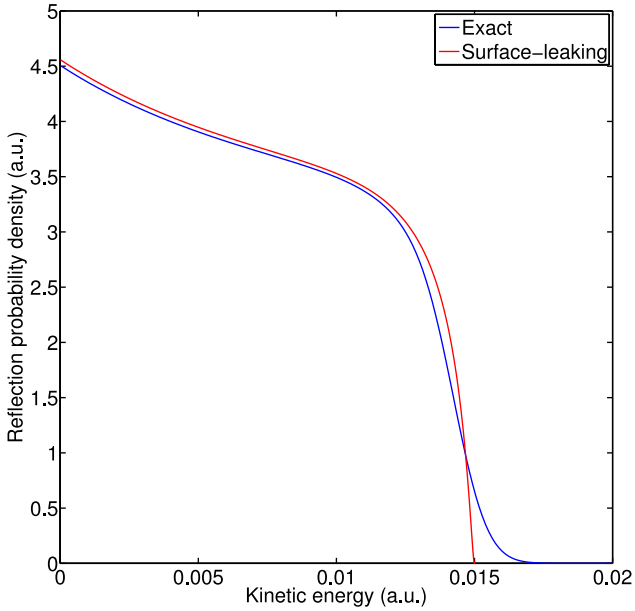

FIG. 4. Model #1: Reflection probability density for the bath states as a function of outgoing kinetic energy according to both exact dynamics and the surface-leaking algorithm. The incoming kinetic energy is 0.015 a.u., the nuclear mass is 100 000 a.u., and $\Gamma(0)$ is 10^{-4} a.u. Note the good agreement.

the accuracy of the SL algorithm. Overall, the SL algorithm performs well for this trivial problem.

2. Dynamics of the system state

Having investigated the dynamics of the bath states, we now turn our attention to transmission and reflection along the system state. Fig. 5 explores the performance of surface-leaking over a wide range of incoming kinetic energies (plotting transmission and reflection probability on the system state, $\Gamma(0) = 10^{-4}$ a.u.). Fig. 6 plots transmission and reflection as a function of $\Gamma(0)$ (keeping the incoming kinetic energy equal to 0.025 a.u.). In both figures, surface-leaking agrees with exact quantum dynamics, further confirming that surface-leaking is the correct approach for this class of problems. As a point of comparison, in Fig. 5 we also plot results from a full FSSH simulation with 10 discretized baths states (as averaged over 2000 trajectories). With only 10 bath states, the FSSH results agree with exact quantum results and surface-leaking results for large incoming kinetic energy where only transmission is significant, but FSSH cannot recover the correct branching ratios for small incoming kinetic energy with only 10 bath states. Instead of a monotonic decline, notice the interesting oscillations in the FSSH reflection probabilities as a function of incoming kinetic energy. These FSSH oscillations can be understood as follows. First, if a frustrated hop is encountered, an incoming FSSH trajectory will follow the active adiabatic PES and "leak" into the bath and produce a small reflection probability. Second, while frustrated hops correspond to energies with too small a reflection probability, there are other energies for which FSSH predicts a reflection probability that is too large—these overestimates must be caused by the over-coherence of FSSH. With this rationale in mind, one would expect to find sharp oscillations in FSSH reflection branching ratios as a function of incoming kinetic energy no matter how many bath states are assumed. As such, beyond computational efficiency, the surface-leaking algorithm has some obvious advantages over FSSH when dealing with a true continuum of electronic states.

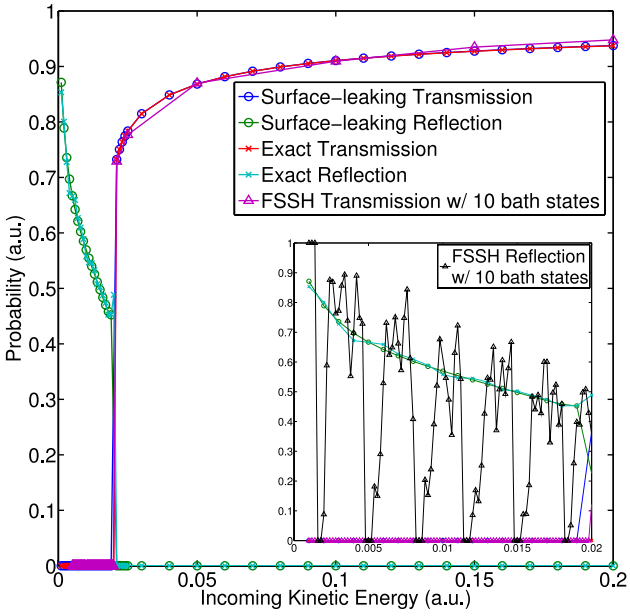

FIG. 5. Model #1: Surface-leaking and exact transmission and reflection probabilities on the system state as a function of incoming kinetic energy. $\Gamma(0)$ is 10^{-4} a.u. Note the good agreement. In this figure, we also plot results using the FSSH algorithm for a bath of 10 electronic states. In the inset, we plot reflection data for FSSH with 10 states. Clearly, at low velocity, SL-FSSH outperforms a full FSSH calculation with only 10 states. See text for more detail.

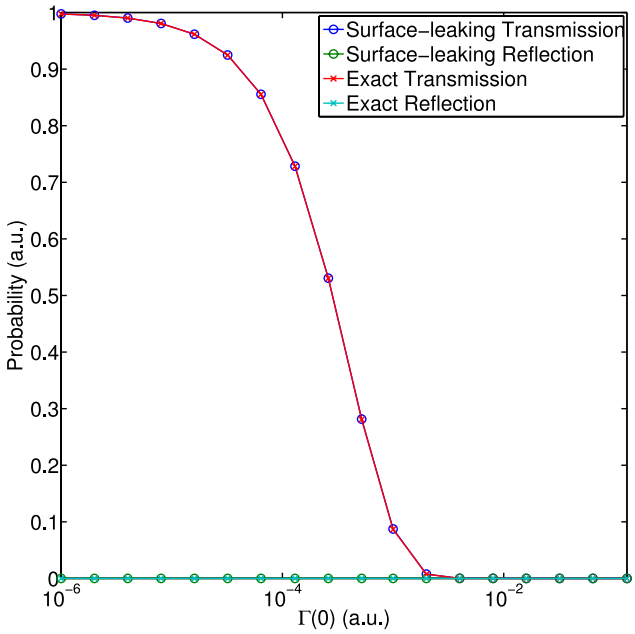

FIG. 6. Model #1: Surface-leaking and exact transmission and reflection probabilities on system state as a function of $\Gamma(0)$. The incoming kinetic energy is 0.025 a.u. Note the good agreement.

B. Models #2 and #3: Two system states with one couples to a set of bath states

Having investigated the bare surface-leaking model, let us now consider the SL-FSSH model and add another system state to the Hamiltonian in Model #1. This change will allow for the possibility of some coherent non-adiabatic dynamics in addition to electronic relaxation. The Hamiltonians for two new models (#2, #3) are as follows:

$$V_{11}(x) = A\tanh(Bx), \tag{22a}$$

$$V_{22}(x) = -V_{11}(x), \tag{22b}$$

$$V_{21}(x) = V_{12}(x) = C\exp(-Dx^2), \tag{22c}$$

$$U(x) = 0.5K\left(\tanh(x+15) + \tanh(15-x)\right), \tag{22d}$$

where $A = 0.01$, $B = 1.6$, $C = 0.005$, $D = 1.0$, and K is a constant defined in the same manner as C in Eq. (20), and all in atomic units.

For both model problems, the system consists of two diabatic states: a donor state (Eq. (22a)) and an acceptor state (Eq. (22b)), and the coupling between them is Eq. (22c). For both model problems, the donor state is coupled to a set of bath states, and the system-bath coupling is shown in Eq. (22d). The manifold of bath states will be different for the two models. For

Model #2, the set of bath states is

$$V_{bath}^{(2)}(x) = V_{22}(x) = -A\tanh(Bx) \tag{23}$$

while for Model #3, the set of bath states is

$$V_{bath}^{(3)}(x) = V_{11}(x) = A\tanh(Bx). \tag{24}$$

Thus, one can think of Model #2 as the donor state coupled to a set of nonparallel bath states, while the set of bath state is parallel to the donor state in Model #3. A set of 6 total diabatic PESs are shown in Figs. 1(b) and 1(c) for Models #2 and #3, respectively.

For these simulations, following Tully's original paper,[42] the mass of the nucleus is set to 2000 a.u. and the simulation is incoming from the left on V_{11}. To keep the calculations as simple as possible (without worrying representation unnecessarily), we will focus on the system populations only and we will not calculate bath distributions. Finally, it is important to note that, in the wide band limit, Models #2 and #3 are effectively identical; indeed, the SL calculations are exactly identical. For this reason, we will show only results from Model #3 in this section. To explore the differences between Models #2 and #3, see Sec. IV C where we report results beyond the wide band approximation.

Fig. 7 shows the FSSH (with no bath), SL-FSSH, and exact results for transmission probability along the system state as a function of incoming kinetic energy. $\Gamma(0)$ is 10^{-4} a.u. The overall agreement between SL-FSSH and exact dynamics is excellent over a wide range of incoming kinetic energies. The fact that SL-FSSH and FSSH have the same overall shape seemingly confirms the notion that the relaxation into the bath does not change the nature of the surface hopping. Notice that, as the incoming kinetic energy grows, the fraction of population remaining in the system increases, as it must (since the particle spends less time leaking into the bath).

Fig. 8 plots transmission as a function of $\Gamma(0)$. The incoming kinetic energy is 0.2 a.u. Note here that, for FSSH (as opposed to SL-FSSH) calculations, the system is not coupled to a bath, so that all FSSH results are independent of $\Gamma(0)$. The agreement between SL-FSSH and exact dynamics is again excellent. As one would expect, transmission on both system states decreases as $\Gamma(0)$ increases—because larger $\Gamma(0)$ leads to more relaxation into the bath. When $\Gamma(0)$ is large enough, no population survives on the system before the nucleus transmits to the right. One interesting feature of Fig. 8 is the competition between surface hopping and surface leaking. When $\Gamma(0)$ is small, the transmission on the upper system state is larger than that on the lower system state. As $\Gamma(0)$ increases, however, the transmission on the upper system state decreases faster than on the lower system state, and around $\Gamma(0) = 10^{-3}$ a.u., the transmission on the upper system state surprisingly becomes smaller than transmission on the lower system state. This relative change in branching ratios occurs because it is the population on diabat 1 alone that leaks into the bath. Thus, on the one hand, the wavepacket transmitting on the upper state is always moving approximately along V_{11} and is constantly decaying; on the other hand, the wavepacket that transmits on lower state moves approximately along V_{22} after it leaves the coupling region, so that decay ceases in time.

Overall, the excellent agreement in both figures between SL-FSSH and exact dynamics suggests the SL-FSSH algorithm is viable in dealing with both irreversible electronic relaxation and short-time coherent non-adiabatic processes.

IV. DISCUSSION

There are now a few items above worth discussing in detail.

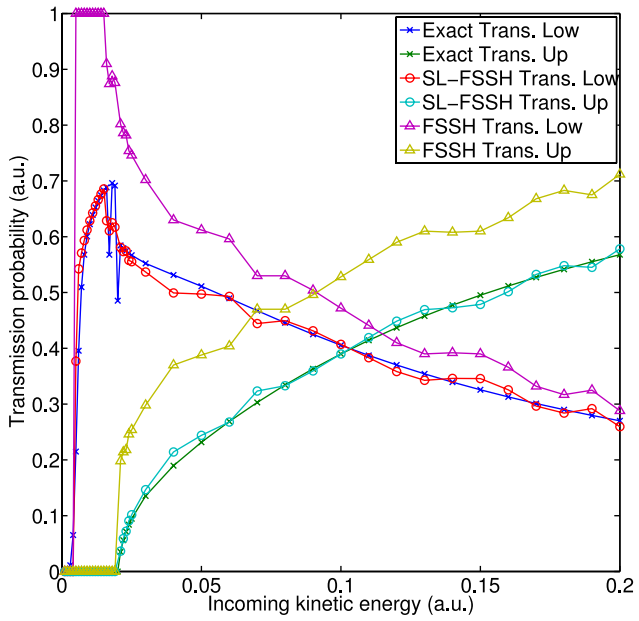

FIG. 7. Model #3: FSSH, SL-FSSH, and exact results for transmission probability on the system state as a function of incoming kinetic energy. $\Gamma(0)$ is 10^{-4} a.u. Note the good agreement.

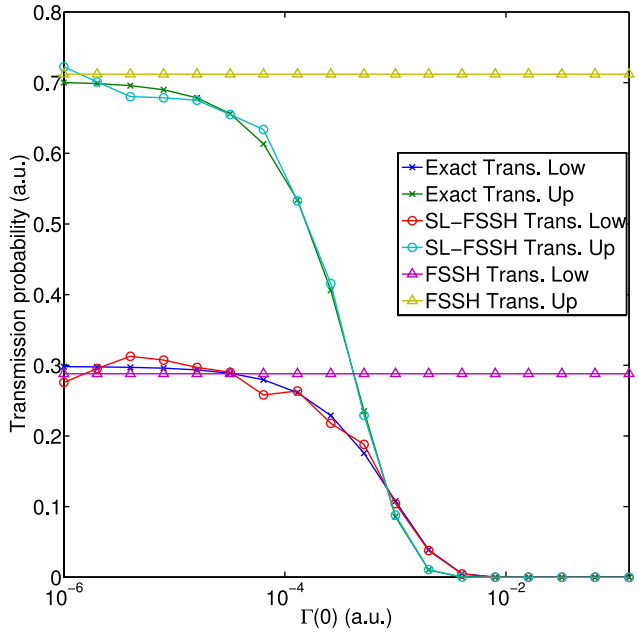

FIG. 8. Model #3: FSSH, SL-FSSH and exact results for transmission probability on the system state as a function of $\Gamma(0)$. The incoming kinetic energy is 0.2 a.u. Note the good agreement.

A. Decoherence: Averaging over an initial Wigner wavepacket

Recall the oscillations in transmission probabilities in Fig. 3. The oscillations exist for outgoing kinetic energy less than 0.02 a.u. A transmission kinetic energy of 0.02 a.u. is special because, if one follows the corresponding diabatic bath for $x \to -\infty$, one finds that the corresponding reflecting wavepacket should have outgoing kinetic energy equal 0 a.u. Thus, this is a special bath state. (See Fig. 9 for a schematic view of the relevant wavepacket dynamics.) For bath states below this special bath state (with less potential energy), reflection is energetically allowed. But for bath states above this special bath state (with more potential energy), reflection is not energetically allowed. So any wavepacket attempting to reflect on such a diabat asymptotically must turn around and transmit to the right instead. In such a case, for a wavepacket wide enough in position space, one expects to find interference between directly transmitting wavepacket and the wavepacket that bounces back and forth. Such interference leads to the oscillations in Fig. 3.

The physics described above has an analogue in the surface-leaking algorithm, but in a slightly different form. Because Γ does not keep track of the coherence between wavepackets on different diabats, one does not find the oscillations in transmission in Fig. 3. However, one does find a big step function at the 0.02 a.u. kinetic energy threshold. (The peak in SL transmission in Fig. 3 at 0.005 a.u. kinetic energy is the result of the classical nucleus slowing down as it turns around to reflect; during this long time period, there is a lot of leakage into the bath.)

Now, in principle, the transmission oscillation in Fig. 3 should vanish if we average over a wavepacket that is wide enough in momentum space. Such initial conditions correspond to an incoming wavepacket that is narrow in position space and therefore the two transmitting wavepackets will exit the coupling region at different times with no interference. In such a case, the SL should be able to recover the exact results because there is no coherence in the dynamics—unlike FSSH,[79] SL has no decoherence or multiple crossing problem.

To prove this point, see the averaged results in Fig. 10. For the exact quantum calculation, we calculate results for plane waves with different incoming momenta and we average all resulting data over a Gaussian distribution

$$\overline{|t_l|^2} = \sum_p |t_l(p)|^2 \, N \exp\left(-\frac{(p-p_0)^2}{2\sigma^2}\right) \Delta p. \tag{25}$$

Here, l is the index for a bath transmission channel, N is a normalization constant, p is the incoming momentum, p_0 is the average momentum of the wavepacket, σ is the width of wavepacket in momentum space, and $|t_l(p)|^2$ represents the result transmission probability on state l when the incoming momentum is p. For the surface-leaking algorithm, we sample the initial momentum from the same Gaussian distribution as in Eq. (25). We invoke 2000 trajectories and set $\sigma = 1$. Note that, after averaging, surface-leaking and exact dynamics are in quite good agreement. (There is still a small disagreement in the peak position; we suspect this is a nuclear tunneling effect.)

B. The mass dependence of the bath dynamics

In Sec. III, we saw that the surface-leaking recovers exact quantum dynamics for system population when the mass of nucleus is either 2000 a.u. or 100 000 a.u. However, as the mass of nucleus becomes smaller, quantum effects (especially tunneling) become important when we calculate the population

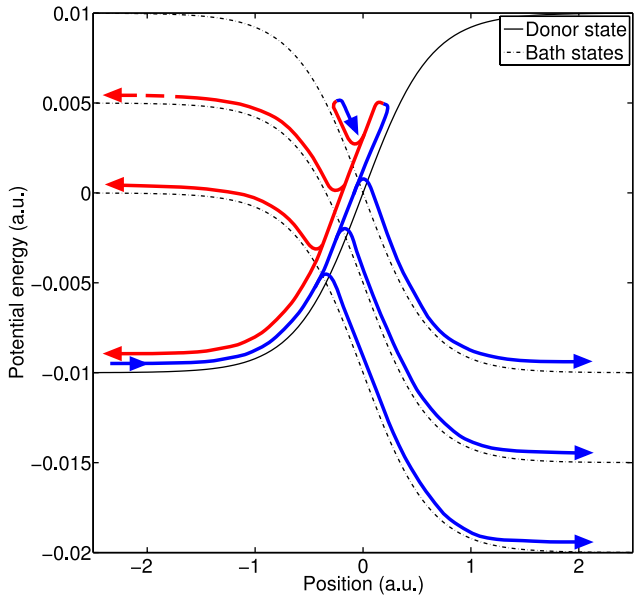

FIG. 9. Model #1: Schematic figure showing the dynamics of population leaking associated with a nucleus whose incoming kinetic energy is 0.015 a.u. The blue paths denote rightward wavepackets and the red paths denote leftward wavepackets. The dash red path for reflection (at potential energy equals 0.005 a.u.) signifies that the asymptotic outgoing kinetic energy is 0 a.u.

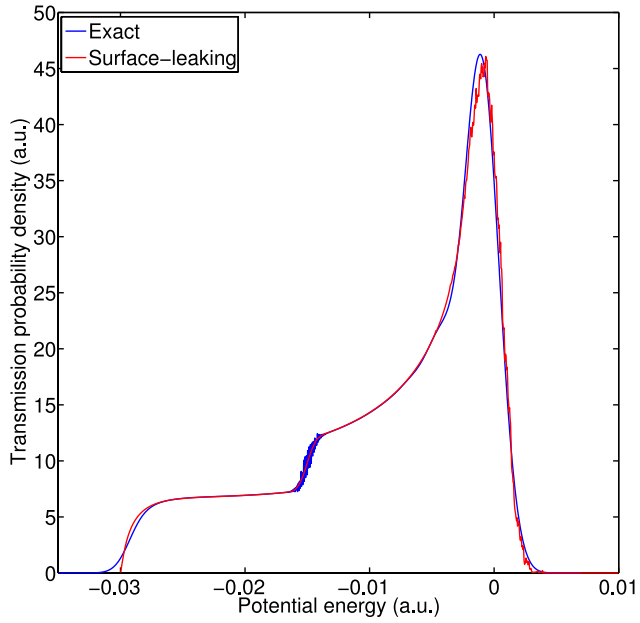

FIG. 10. Model #1: Transmission probability density for the bath states as a function of potential energy of outgoing channels according to both exact dynamics and surface-leaking algorithm. The incoming kinetic energy for surface-leaking is 0.015 a.u., the mass of nucleus is 100 000 a.u. and $\Gamma(0)$ is 10^{-4} a.u. Both exact and surface-leaking results are averaged over an incoming Gaussian wavepacket distribution (according to Eq. (25) with $\sigma = 1$). Note the good agreement.

distribution in the bath states. In Fig. 11, we replot the calculation from Fig. 2, only now we change the nuclear mass to 2000 a.u. For comparison, we include data from mass equals 100 000 a.u. (Fig. 2). Even though the overall shape still matches, it is evident that the SL errors become larger as the mass decreases.

C. Wide band approximation

In all the SL-FSSH simulations above, we have assumed that the energy range of the bath is infinite so the relaxation process follows Fermi's Golden Rule with rate Γ. Correspondingly, for the exact dynamics calculations, we have always included enough bath states so that the system is completely embedded in a broad bath. While these approximations are useful and lead to simple physics, the wide band approximation is not always true, and it will be interesting to see what happens if we go beyond the wide band approximation.

When the wide band approximation breaks down, Fermi's Golden Rule is no longer valid, and the system does not decay exponentially into the bath. Instead, only a fraction of the system decays into the bath as determined by the projection of the system state into the eigenstates of the Hamiltonian. This projection can be calculated from the imaginary part of the Green's function, also known as the spectral density.

The Green's function can be written as

$$G(E) = \frac{1}{i\hbar}\lim_{\varepsilon\to 0}\int_0^\infty dt\,\langle\psi(0)|\psi(t)\rangle\exp\left(i(E+i\varepsilon)t/\hbar\right). \quad (26)$$

Let the wave function $|\psi(0)\rangle$ be expressed in an adiabatic basis as

$$|\psi(0)\rangle = \sum_j c_j\,|\phi\rangle, \quad (27)$$

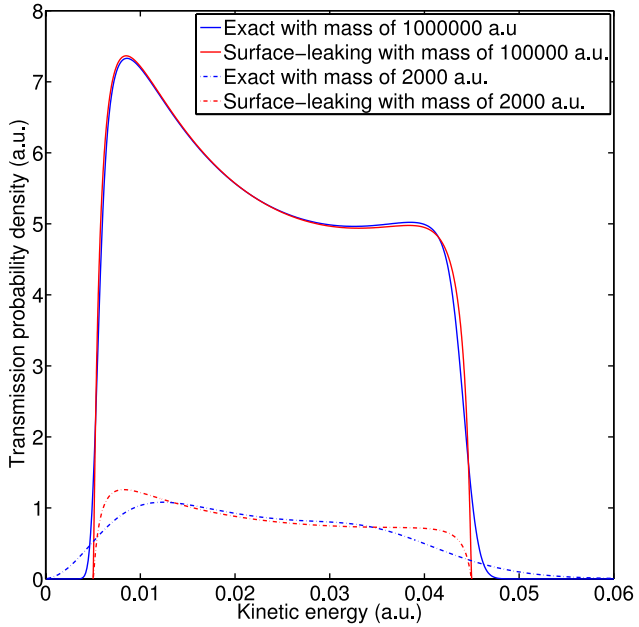

FIG. 11. Model #1: Transmission probability density for the bath states as a function of outgoing kinetic energy according to exact dynamics and the surface-leaking algorithm. The incoming kinetic energy is 0.025 a.u., $\Gamma(0)$ is 10^{-4} a.u. and the mass of nucleus is 100 000 a.u. or 2000 a.u. (For mass equals to 100 000 a.u., the data are the same as in Fig. 2.) As mass is reduced, surface-leaking results differ more and more from the exact results.

where c_j are the amplitudes. The Green's function becomes

$$\begin{aligned}
G(E) &= \frac{1}{i\hbar}\lim_{\varepsilon\to 0}\int_0^\infty dt\sum_j |c_j|^2 \\
&\quad\times\exp\left(-iE_jt/\hbar + i(E+i\varepsilon)t/\hbar\right) \\
&= \frac{1}{i\hbar}\lim_{\varepsilon\to 0}\sum_j |c_j|^2\frac{-\hbar}{i(E-E_j+i\varepsilon)} \\
&= \lim_{\varepsilon\to 0}\sum_j \frac{|c_j|^2}{E-E_j+i\varepsilon} \\
&= \mathrm{PP}\int_{-\infty}^{\infty} dE'\frac{\rho(E')|c(E')|^2}{E-E'} \\
&\quad - i\pi\int_{-\infty}^{\infty} dE'\rho(E')|c(E')|^2\delta(E-E') \\
&= \mathrm{PP}\int_{-\infty}^{\infty} dE'\frac{\rho(E')|c(E')|^2}{E-E'} - i\pi\rho(E)|c(E)|^2. \quad (28)
\end{aligned}$$

Here, PP means the Cauchy principal value and the following two transformations have been used:

$$\sum_j \to \int dE\rho(E), \quad (29)$$

$$\lim_{\varepsilon\to 0}\frac{1}{x+i\varepsilon} \to \mathrm{PP}\frac{1}{x} - i\pi\delta(x). \quad (30)$$

Thus, the spectral density is

$$\rho(E)|c(E)|^2 = \frac{-\mathrm{Im}(G(E))}{\pi}. \quad (31)$$

For a model—with one discrete state (E_0) coupled linearly to a set of bath states—the Green's function is

$$G(E) = \frac{1}{E - E_0 - \sum_k \frac{|V|^2}{E-E_k}}. \quad (32)$$

The self-energy in the above equation can be calculated as

$$\begin{aligned}
\sum_k \frac{|V|^2}{E-E_k} &= \lim_{\varepsilon\to 0}\sum_k \frac{|V|^2}{E-E_k+i\varepsilon} \\
&= \mathrm{PP}\int_{-w}^{w} dE_k\rho(E_k)\frac{|V|^2}{E-E_k} - i\pi|V|^2\rho(E) \\
&= \frac{\Gamma}{2\pi}\ln\left(\frac{E+w}{w-E}\right) - \frac{i\Gamma}{2} \quad (33)
\end{aligned}$$

where w is the half-width of bath and $\Gamma = 2\pi\rho(E)|V|^2$. Thus, the relative proportion of the system state inside of the band is

$$\begin{aligned}
F_{inside} &\equiv -\int_{-w}^{w}\frac{\mathrm{Im}(G(E))}{\pi} \\
&= \frac{1}{\pi}\int_{-w}^{w} dE\frac{2\Gamma}{4\left[E - E_0 - \frac{\Gamma}{2\pi}\ln\left(\frac{E+w}{w-E}\right)\right]^2 + \Gamma^2}. \quad (34)
\end{aligned}$$

For SL-FSSH, to account for the band width, Eq. (15) should be rewritten as

$$L_i(\mathbf{R}) = \frac{F_{inside}\Gamma_i(\mathbf{R})\Delta t}{\hbar}. \quad (35)$$

In Fig. 12, we plot the transmission probability for system states as a function of bath width for Model #2. $\Gamma(0)$ is 10^{-4} a.u. and the incoming kinetic energy is 0.2 a.u. We plot exact scattering results with and without the bath states, as well as

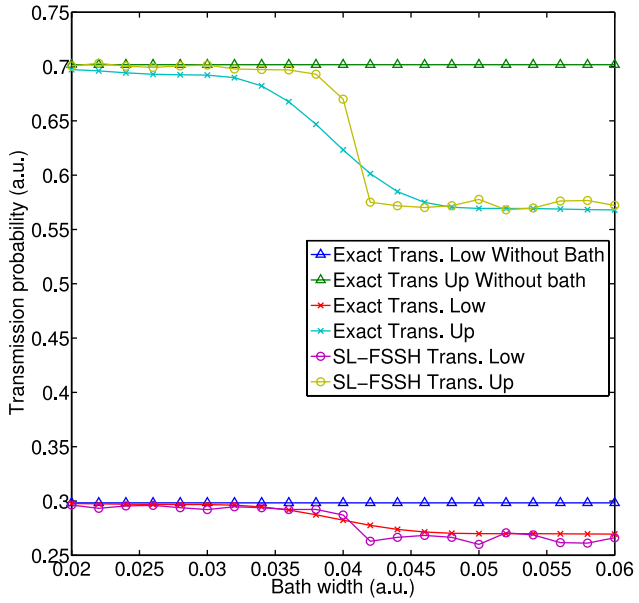

FIG. 12. Model #2: Transmission results for the system channels as a function of bath width. The incoming kinetic energy is 0.2 a.u., the nuclear mass is 2000 a.u., and $\Gamma(0)$ is 10^{-4} a.u. SL-FSSH results are averaged over 40 000 trajectories. Note that SL-FSSH agrees with exact dynamics in the limit of very wide and very narrow band, but the crossover is not quantitative at all.

SL-FSSH. SL-FSSH converges to the exact results in the limit of very wide and very narrow bands. However, in between these two limits, SL-FSSH cannot recover the correct gradual transition; instead SL-FSSH predicts a steep jump. This failure indicates that our approximation for dynamics beyond the wide band limit is still too extreme to be quantitative accurate.

Results for Model #3 are shown in Fig. 13. $\Gamma(0)$ is 10^{-4} a.u. and the incoming kinetic energy is 0.2 a.u. Just as we saw

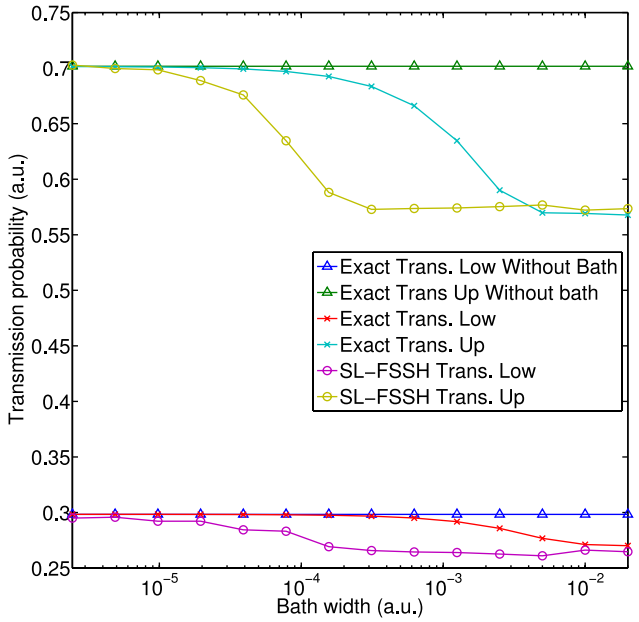

FIG. 13. Model #3: Transmission results for the system channels as a function of bath width. The incoming kinetic energy is 0.2 a.u., the nuclear mass is 2000 a.u., and $\Gamma(0)$ is 10^{-4} a.u. SL-FSSH results are averaged over 40 000 trajectories. Note that SL-FSSH agrees with exact dynamics in the limit of very wide and very narrow band, but the crossover is not quantitative at all.

for Model #2, we recover the correct dynamics in the two extreme limits: very wide and very narrow bands. However, for intermediate value of Γ, the agreement between SL-FSSH and exact dynamics is far worse for Model #3 than for Model #2. This failure can be explained by the length of time (T) spent by the donor system state interacting with the bath. For Model #2, the crossings are sharper and T is smaller; for Model #3, the bath follows the donor state and T is large. In the future, Model #3 will be a good test case for benchmarking an improved SL-FSSH scheme that goes beyond the wide band limit.

V. CONCLUSION

In this paper, we have proposed a simple surface-leaking fewest-switches surface hopping (SL-FSSH) algorithm that combines Tully's FSSH and Preston's SL algorithms. We have benchmarked SL-FSSH on three similar but different system-bath model problems with various parameters. By comparing SL-FSSH results versus exact scattering quantum calculations, we have shown that the algorithm works well over a wide range of nuclear velocities and system-bath coupling strengths in the wide band limit. When we go beyond the wide band approximation, we find only partial success and further improvements to the algorithm will be needed in order to recover the details of the transition between a wide and narrow band of bath states. Corrections should be possible in the future. Considering the low cost of the SL-FSSH algorithm, the prevalence of wide bands, and the ubiquitousness of both relaxation and short-time coherent non-adiabatic processes, SL-FSSH should be useful in a wide variety of applications. In particular, one obvious application would be molecular processes on weakly coupled metal surfaces.[80]

ACKNOWLEDGMENTS

J.E.S. thanks Neil Shenvi and Misha Galperin for very helpful discussions. This material is based upon work supported by the (U.S.) Air Force Office of Scientific Research (USAFOSR) PECASE award under AFOSR Grant No. FA9950-13-1-0157. J.E.S. acknowledges a Cottrell Research Scholar Fellowship and a David and Lucille Packard Fellowship.

APPENDIX: EXACT QUANTUM CALCULATION

Let us now describe how we have calculated exact quantum scattering results with ~1000 electronic states.[81] Our notation will be as follows. For indices of electronic states, α is an index for reflecting states, β is an index for transmitting states, and ε is an index for either. For quantity labeling, a superscript of (r) refers to reflections related quantities and (t) for transmission, superscript of $(left)$ and $(right)$ are for quantities evaluated on the left and right sides of the region of interest, respectively, a subscript of inc refers to quantities attached to the incoming electronic state. For physical quantities, $\mathbf{H}$ denotes the Hamiltonian, $|\phi\rangle$ is diabatic electronic state, k is a wave number, and V is the potential energy.

Exact quantum results are calculated by solving equation

$$(\mathbf{H} - E_0)\,|\psi(x)\rangle = 0, \tag{A1}$$

where $\mathbf{H}$ is the Hamiltonian, E_0 is initial total energy, and $|\psi(x)\rangle$ is the wave function defined in three regions. Region I is on the left of region of interest, Region II is the region of interest, and Region III is on the right of region of interest. (The region of interest is where all coupling occurs.) The wave function can be written as

$$|\psi(x)\rangle = \begin{cases} e^{ik_{inc}x}|\phi_{inc}\rangle + \sum_\alpha r_\alpha e^{-ik_\alpha^{(r)}x}|\phi_\alpha\rangle & \text{Region I,} \\ \sum_\varepsilon c_\varepsilon(x)|\phi_\varepsilon\rangle & \text{Region II,} \\ \sum_\beta t_\beta e^{ik_\beta^{(t)}x}|\phi_\beta\rangle & \text{Region III.} \end{cases} \tag{A2}$$

Here, $k_{inc} = \sqrt{2M(E_0 - V_{inc}^{(left)})}/\hbar$ where M is the nuclear mass, $k_\alpha^{(r)} = \sqrt{2M(E_0 - V_\alpha^{(left)})}/\hbar$, and $k_\beta^{(t)} = \sqrt{2M(E_0 - V_\beta^{(right)})}/\hbar$. r_ε and t_ε are reflection and transmission amplitudes, respectively, on state ε, and $c_\varepsilon(x)$ are amplitudes for the wave function in the interior region of interest (region II). The sum over α (β) includes all electronic states such that the $k_\alpha^{(r)}$ ($k_\beta^{(t)}$) are real, i.e., those electronic states that are energetically accessible.

Clearly, the wave function $|\psi(x)\rangle$ has four parts: (1) an asymptotically incoming wave, (2) an asymptotically reflecting wave, (3) an asymptotically transmitting wave, (4) an interior wave function. The first three components are localized plane waves. For a fixed incoming wave, the challenge is to compute the other 3 unknown variables by solving Eq. (A1).

We solve Eq. (A1) using a grid in position space with the kinetic operator in Hamiltonian expressed by a 5-stencil finite difference matrix. Eq. (A1) is then rearranged into the form

$$(\mathbf{H} - E_0)(|\psi(x)\rangle - |\psi_{inc}(x)\rangle) = -(\mathbf{H} - E_0)|\psi_{inc}(x)\rangle, \tag{A3}$$

where $|\psi_{inc}(x)\rangle$ is the known incoming wave and $|\psi(x)\rangle - |\psi_{inc}(x)\rangle$ is the unknown vector that must be solved.

We use a two-dimensional basis for the Hamiltonian, $|\varepsilon, x\rangle = |\phi_\varepsilon\rangle \otimes |x\rangle$. Here, ε labels each diabatic electronic state, $\varepsilon = 1, 2, \ldots, N_\varepsilon$ where N_ε is the total number of electronic states. We set x as the index for a grid in position space, $x = -2, -1, \ldots, N_x + 2, N_x + 3$ where N_x is the total number of grid point in the region of interest. The bra space of the Hamiltonian is defined as

$$\{\langle 1,1|, \langle 1,2|, \ldots, \langle 1,N_x|, \langle 2,1|, \langle 2,2|, \ldots, \langle N_\varepsilon, N_x|, \langle 1,0|, \langle 2,0|, \ldots, \langle N_\alpha, 0|, \langle 1, N_x+1|, \langle 2, N_x+1|, \ldots, \langle N_\beta, N_x+1|\}. \tag{A4}$$

The ket space of the Hamiltonian is defined as

$$\{|1,1\rangle, |1,2\rangle, \ldots, |1,N_x\rangle, |2,1\rangle, |2,2\rangle, \ldots, |N_\varepsilon, N_x\rangle, |r_1\rangle, |r_2\rangle, \ldots, |r_{N_\alpha}\rangle, |t_1\rangle, |t_2\rangle, \ldots, |t_{N_\beta}\rangle\}. \tag{A5}$$

Here, N_α and N_β are the total number of states that are energetically allowed for reflection and transmission, respectively. $|r_\varepsilon\rangle$ is a basis function for a reflecting state defined as

$$|r_\varepsilon\rangle \equiv e^{2ik_\varepsilon^{(r)}\Delta x}|\varepsilon, -2\rangle + e^{ik_\varepsilon^{(r)}\Delta x}|\varepsilon, -1\rangle + |\varepsilon, 0\rangle, \tag{A6}$$

where Δx is the bin size of position grid. Similarly, $|t_\varepsilon\rangle$ is a basis function for a transmitting state defined as

$$|t_\varepsilon\rangle \equiv |\varepsilon, N_x+1\rangle + e^{ik_\varepsilon^{(t)}\Delta x}|\varepsilon, N_x+2\rangle + e^{2ik_\varepsilon^{(t)}\Delta x}|\varepsilon, N_x+3\rangle. \tag{A7}$$

Note that the bra and ket spaces are the same for the first $N_\varepsilon N_x$ dimensions but different for the last $N_\alpha + N_\beta$ dimensions. While the ket basis contains transmitting and reflecting wave, the bra basis contains the grid points $\langle 0|$ and $\langle N_x + 1|$ to encode the boundary.

In the basis above, the Hamiltonian is not symmetric and can be broken down by region as

$$\mathbf{H} = \begin{pmatrix} \mathbf{H}_{II,II} & \mathbf{H}_{II,I} & \mathbf{H}_{II,III} \\ \mathbf{H}_{I,II} & \mathbf{H}_{I,I} & 0 \\ \mathbf{H}_{III,II} & 0 & \mathbf{H}_{III,III} \end{pmatrix}. \tag{A8}$$

$\mathbf{H}_{II,II}$ is the Hamiltonian for the region of interest while other blocks involve the boundary. $\mathbf{H}_{II,II}$ has dimensionality of $N_\varepsilon N_x \times N_\varepsilon N_x$ and the ket space is the same as bra space. The matrix elements of $\mathbf{H}_{II,II}$ are defined as

$$\langle \varepsilon_1, x_1|\mathbf{H}_{II,II}|\varepsilon_2, x_2\rangle = C\left[\left(\frac{5}{2} + \frac{V_{\varepsilon_1}(x_1)}{C}\right)\delta_{x_1,x_2} - \frac{4}{3}\delta_{x_1,x_2\pm1} + \frac{1}{12}\delta_{x_1,x_2\pm2}\right]\delta_{\varepsilon_1,\varepsilon_2} + U_{\varepsilon_1,\varepsilon_2}(x_1)\delta_{x_1,x_2}. \tag{A9}$$

Here, δ is the Kronecker delta, $U_{\varepsilon_1,\varepsilon_2}$ is the electronic coupling between states ε_1 and ε_2, and the constant factor $C = \hbar^2/(2M\Delta x^2)$, where M is the nuclear mass. $\mathbf{H}_{I,I}$, $\mathbf{H}_{II,I}$, and $\mathbf{H}_{I,II}$ are the matrix elements at the boundary for the reflecting wave and have dimensionality of $N_\alpha \times N_\alpha$, $N_\varepsilon N_x \times N_\alpha$, and $N_\alpha \times N_\varepsilon N_x$, respectively. $\mathbf{H}_{I,I}$ is defined as

$$\langle \varepsilon, 0|\mathbf{H}_{I,I}|r_\alpha\rangle = C\left(\frac{1}{12}e^{2ik_\varepsilon^{(r)}\Delta x} - \frac{4}{3}e^{ik_\varepsilon^{(r)}\Delta x} + \frac{5}{2} + \frac{V_\varepsilon(0)}{C}\right)\delta_{\varepsilon,\alpha}. \tag{A10}$$

$\mathbf{H}_{II,I}$ is defined as

$$\langle \varepsilon, x|\mathbf{H}_{II,I}|r_\alpha\rangle = C\left[\left(\frac{1}{12}e^{ik_\varepsilon^{(r)}\Delta x} - \frac{4}{3}\right)\delta_{x,1} + \frac{1}{12}\delta_{x,2}\right]\delta_{\varepsilon,\alpha}. \tag{A11}$$

$\mathbf{H}_{I,II}$ is defined as

$$\langle \varepsilon_1, 0|\mathbf{H}_{I,II}|\varepsilon_2, x\rangle = C\left(-\frac{4}{3}\delta_{x,1} + \frac{1}{12}\delta_{x,2}\right)\delta_{\varepsilon_1,\varepsilon_2}. \tag{A12}$$

$\mathbf{H}_{\mathrm{III,III}}$, $\mathbf{H}_{\mathrm{II,III}}$, and $\mathbf{H}_{\mathrm{III,II}}$ are the matrix elements at the boundary for the transmitting wave and have dimensionality of $N_\beta \times N_\beta$, $N_\varepsilon N_x \times N_\beta$, and $N_\beta \times N_\varepsilon N_x$, respectively. $\mathbf{H}_{\mathrm{III,III}}$ is defined as

$$\langle \varepsilon, N_x+1 | \mathbf{H}_{\mathrm{III,III}} | t_\beta \rangle = C\left(\frac{1}{12}e^{2ik_\varepsilon^{(t)}\Delta x} - \frac{4}{3}e^{ik_\varepsilon^{(t)}\Delta x} + \frac{5}{2} + \frac{V_\varepsilon(N_x+1)}{C}\right)\delta_{\varepsilon,\beta}. \tag{A13}$$

$\mathbf{H}_{\mathrm{II,III}}$ is defined as

$$\langle \varepsilon, x | \mathbf{H}_{\mathrm{II,III}} | t_\beta \rangle = C\left[\left(\frac{1}{12}e^{ik_\varepsilon^{(t)}\Delta x} - \frac{4}{3}\right)\delta_{x,N_x} + \frac{1}{12}\delta_{x,N_x-1}\right]\delta_{\varepsilon,\beta}. \tag{A14}$$

$\mathbf{H}_{\mathrm{III,II}}$ is defined as

$$\langle \varepsilon_1, N_x+1 | \mathbf{H}_{\mathrm{III,II}} | \varepsilon_2, x \rangle = C\left(-\frac{4}{3}\delta_{x,N_x} + \frac{1}{12}\delta_{x,N_x-1}\right)\delta_{\varepsilon_1,\varepsilon_2}. \tag{A15}$$

The incoming wave function is chosen as

$$|\psi_{inc}(x)\rangle = e^{-2ik_{inc}\Delta x}|inc,-2\rangle + e^{-ik_{inc}\Delta x}|inc,-1\rangle + |inc,0\rangle. \tag{A16}$$

The elements of $(E_0 - \mathbf{H})|\psi_{inc}(x)\rangle$ are evaluated as

$$\langle \varepsilon, x | (E_0 - \mathbf{H}) | \psi_{inc}(x)\rangle = C\left[\left(-\frac{5}{2} + \frac{4}{3}e^{-ik_{inc}\Delta x} - \frac{1}{12}e^{-2ik_{inc}\Delta x} + \frac{E_0 - V_{inc}}{C}\right)\delta_{x,0} + \left(\frac{4}{3} - \frac{1}{12}e^{-ik_{inc}\Delta x}\right)\delta_{x,1} - \frac{1}{12}\delta_{x,2}\right]\delta_{\varepsilon,inc}. \tag{A17}$$

This completes our description of how the Hamiltonian is constructed. In practice, Eq. (A3) is solved numerically by using Intel MKL PARDISO[82] solver which is a parallel direct sparse solver. Taking advantage of the large sparsity of the Hamiltonian, the sparse solver minimizes the memory needed to storing the matrix as well as the CPU time for solving Eq. (A3). As such, the sparse solver makes it possible to include thousands of electronic states in the bath and grid points in position space and solve Eq. (A3) in a reasonable time. For instance, the calculation associated with results in Fig. 13 has 501 discretized electronic states in the bath combined with 6000 grid points in region II ($[-30, 30]$) a.u., and the CPU time is less than 4 min (the real time is 1 min by running in parallel with 4 cores).

Reflection probabilities are then found by renormalizing the amplitudes of every channel n according to

$$\left|r_n^{(norm)}\right|^2 = \frac{k_n^{(r)}}{k_{inc}}|r_n|^2. \tag{A18}$$

Transmission amplitudes are renormalized analogously.

[1] R. K. Preston, J. Chem. Phys. **65**, 1589 (1976).
[2] W. H. Miller, J. Chem. Phys. **52**, 3563 (1970).
[3] T. Ogawa and K. Ohno, J. Phys. Chem. A **103**, 9925 (1999).
[4] T. Ogawa and K. Ohno, J. Chem. Phys. **110**, 3773 (1999).
[5] K. Imura, N. Kishimoto, and K. Ohno, J. Phys. Chem. A **106**, 3759 (2002).
[6] S. Falcinelli, P. Candori, M. Bettoni, F. Pirani, and F. Vecchiocattivi, J. Phys. Chem. A **118**, 6501 (2014).
[7] L. S. Cederbaum, J. Zobeley, and F. Tarantelli, Phys. Rev. Lett. **79**, 4778 (1997).
[8] S. Marburger, O. Kugeler, U. Hergenhahn, and T. Möller, Phys. Rev. Lett. **90**, 203401 (2003).
[9] T. Jahnke, A. Czasch, M. Schöffler, S. Schössler, A. Knapp, M. Käsz, J. Titze, C. Wimmer, K. Kreidi, R. Grisenti, A. Staudte, O. Jagutzki, U. Hergenhahn, H. Schmidt-Böcking, and R. Dörner, Phys. Rev. Lett. **93**, 163401 (2004).
[10] N. Sisourat, J. Chem. Phys. **139**, 074111 (2013).
[11] T. Miteva, Y.-C. Chiang, P. Kolorenč, A. I. Kuleff, K. Gokhberg, and L. S. Cederbaum, J. Chem. Phys. **141**, 064307 (2014).
[12] R. S. Berry, Radiat. Res. **59**, 367 (1974).
[13] A. E. Jailaubekov, A. P. Willard, J. R. Tritsch, W.-L. Chan, N. Sai, R. Gearba, L. G. Kaake, K. J. Williams, K. Leung, P. J. Rossky, and X.-Y. Zhu, Nat. Mater. **12**, 66 (2013).
[14] A. Albers, S. Demeshko, S. Dechert, C. T. Saouma, J. M. Mayer, and F. Meyer, J. Am. Chem. Soc. **136**, 3946 (2014).
[15] S. A. Fischer, D. B. Lingerfelt, J. W. May, and X. Li, Phys. Chem. Chem. Phys. **16**, 17507 (2014).
[16] B. R. Landry and J. E. Subotnik, J. Chem. Theory Comput. **10**, 4253 (2014).
[17] R. Long and O. V. Prezhdo, J. Am. Chem. Soc. **136**, 4343 (2014).
[18] T. Nelson, S. Fernandez-Alberti, A. E. Roitberg, and S. Tretiak, Acc. Chem. Res. **47**, 1155 (2014).
[19] J. Liu, A. J. Neukirch, and O. V. Prezhdo, J. Phys. Chem. C **118**, 20702 (2014).
[20] C. A. Schwerdtfeger, A. V. Soudackov, and S. Hammes-Schiffer, J. Chem. Phys. **140**, 034113 (2014).
[21] J. H. Freed, J. Chem. Phys. **49**, 376 (1968).
[22] V. I. Borovkov, I. V. Beregovaya, L. N. Shchegoleva, P. A. Potashov, V. A. Bagryansky, and Y. N. Molin, J. Chem. Phys. **137**, 104305 (2012).
[23] N. D. Almeida and G. Goward, J. Power Sources **268**, 853 (2014).
[24] J. Rantaharju, J. Mareš, and J. Vaara, J. Chem. Phys. **141**, 014109 (2014).
[25] M. Reufer, M. J. Walter, P. G. Lagoudakis, A. B. Hummel, J. S. Kolb, H. G. Roskos, U. Scherf, and J. M. Lupton, Nat. Mater. **4**, 340 (2005).
[26] A. Cannizzo, A. M. Blanco-Rodríguez, A. E. Nahhas, J. Sebera, S. Zális, A. Vlcek, and M. Chergui, J. Am. Chem. Soc. **130**, 8967 (2008).
[27] A. M. Losa, I. F. Galvan, M. L. Sanchez, M. E. Martín, and M. A. Aguilar, J. Phys. Chem. B **112**, 877 (2008).
[28] D.-C. Sergentu, R. Maurice, R. W. A. Havenith, R. Broer, and D. Roca-Sanjuán, Phys. Chem. Chem. Phys. **16**, 25393 (2014).
[29] S. Mai, P. Marquetand, and L. González, J. Chem. Phys. **140**, 204302 (2014).
[30] H.-D. Meyer and W. H. Miller, J. Chem. Phys. **70**, 3214 (1979).
[31] H.-D. Meyer and W. H. Miller, J. Chem. Phys. **72**, 2272 (1980).
[32] G. Stock and M. Thoss, Phys. Rev. Lett. **78**, 578 (1997).
[33] W. H. Miller, J. Phys. Chem. A **113**, 1405 (2009).
[34] H. Kim, A. Nassimi, and R. Kapral, J. Chem. Phys. **129**, 084102 (2008).
[35] A. Nassimi, S. Bonella, and R. Kapral, J. Chem. Phys. **133**, 134115 (2010).
[36] A. Kelly, R. van Zon, J. Schofield, and R. Kapral, J. Chem. Phys. **136**, 084101 (2012).
[37] N. Rekik, C.-Y. Hsieh, H. Freedman, and G. Hanna, J. Chem. Phys. **138**, 144106 (2013).
[38] H. W. Kim and Y. M. Rhee, J. Chem. Phys. **140**, 184106 (2014).
[39] T. J. Martínez, M. Ben-Nun, and R. D. Levine, J. Phys. Chem. **100**, 7884 (1996).

[40]M. Ben-Nun and T. J. Martínez, J. Chem. Phys. **112**, 6113 (2000).
[41]S. Yang, J. D. Coe, B. Kaduk, and T. J. Martínez, J. Chem. Phys. **130**, 134113 (2009).
[42]J. C. Tully, J. Chem. Phys. **93**, 1061 (1990).
[43]W. Dou, A. Nitzan, and J. E. Subotnik, J. Chem. Phys. **142**, 084110 (2015).
[44]J. C. Tully and R. K. Preston, J. Chem. Phys. **55**, 562 (1971).
[45]F. Webster, P. Rossky, and R. Friesner, Comput. Phys. Commun. **63**, 494 (1991).
[46]F. Webster, E. T. Wang, P. J. Rossky, and R. A. Friesner, J. Chem. Phys. **100**, 4835 (1994).
[47]B. J. Schwartz, E. R. Bittner, O. V. Prezhdo, and P. J. Rossky, J. Chem. Phys. **104**, 5942 (1996).
[48]O. V. Prezhdo and P. J. Rossky, J. Chem. Phys. **107**, 825 (1997).
[49]J.-Y. Fang and S. Hammes-Schiffer, J. Chem. Phys. **110**, 11166 (1999).
[50]J.-Y. Fang and S. Hammes-Schiffer, J. Phys. Chem. A **103**, 9399 (1999).
[51]Y. L. Volobuev, M. D. Hack, M. S. Topaler, and D. G. Truhlar, J. Chem. Phys. **112**, 9716 (2000).
[52]A. W. Jasper, M. D. Hack, and D. G. Truhlar, J. Chem. Phys. **115**, 1804 (2001).
[53]M. D. Hack and D. G. Truhlar, J. Chem. Phys. **114**, 2894 (2001).
[54]K. F. Wong and P. J. Rossky, J. Chem. Phys. **116**, 8418 (2002).
[55]K. F. Wong and P. J. Rossky, J. Chem. Phys. **116**, 8429 (2002).
[56]C. Zhu, A. W. Jasper, and D. G. Truhlar, J. Chem. Phys. **120**, 5543 (2004).
[57]C. Zhu, S. Nangia, A. W. Jasper, and D. G. Truhlar, J. Chem. Phys. **121**, 7658 (2004).
[58]A. W. Jasper and D. G. Truhlar, J. Chem. Phys. **123**, 064103 (2005).
[59]N. Shenvi, J. E. Subotnik, and W. Yang, J. Chem. Phys. **134**, 144102 (2011).
[60]J. E. Subotnik and N. Shenvi, J. Chem. Phys. **134**, 024105 (2011).
[61]N. Shenvi, J. E. Subotnik, and W. Yang, J. Chem. Phys. **135**, 024101 (2011).
[62]H. M. Jaeger, S. Fischer, and O. V. Prezhdo, J. Chem. Phys. **137**, 22A545 (2012).
[63]B. R. Landry and J. E. Subotnik, J. Chem. Phys. **137**, 22A513 (2012).
[64]J. E. Subotnik, W. Ouyang, and B. R. Landry, J. Chem. Phys. **139**, 214107 (2013).
[65]T. Nelson, S. Fernandez-Alberti, V. Chernyak, A. E. Roitberg, and S. Tretiak, J. Chem. Phys. **136**, 054108 (2012).
[66]L. Wang and O. V. Prezhdo, J. Phys. Chem. Lett. **5**, 713 (2014).
[67]G. Granucci, M. Persico, and A. Toniolo, J. Chem. Phys. **114**, 10608 (2001).
[68]G. A. Meek and B. G. Levine, J. Phys. Chem. Lett. **5**, 2351 (2014).
[69]S. A. Fischer, C. T. Chapman, and X. Li, J. Chem. Phys. **135**, 144102 (2011).
[70]N. Shenvi, S. Roy, and J. C. Tully, J. Chem. Phys. **130**, 174107 (2009).
[71]N. Shenvi, S. Roy, and J. C. Tully, Science **326**, 829 (2009).
[72]N. Shenvi, J. Schmidt, S. Edwards, and J. Tully, Phys. Rev. A **78**, 022502 (2008).
[73]H. Nakanishi, K. J. M. Bishop, B. Kowalczyk, A. Nitzan, E. A. Weiss, K. V. Tretiakov, M. M. Apodaca, R. Klajn, J. F. Stoddart, and B. A. Grzybowski, Nature **460**, 371 (2009).
[74]N. G. Rey and H. Arnolds, J. Chem. Phys. **135**, 224708 (2011).
[75]H. Petek, J. Chem. Phys. **137**, 091704 (2012).
[76]N. Shenvi and W. Yang, J. Chem. Phys. **137**, 22A528 (2012).
[77]B. R. Landry, M. J. Falk, and J. E. Subotnik, J. Chem. Phys. **139**, 211101 (2013).
[78]To construct a probability density from a finite scattering calculation, one multiplies the probability of a given channel to be occupied by the density of states.
[79]J. E. Subotnik and N. Shenvi, J. Chem. Phys. **134**, 244114 (2011).
[80]G. Floß, G. Granucci, and P. Saalfrank, J. Chem. Phys. **137**, 234701 (2012).
[81]J. E. Subotnik and A. Nitzan, J. Chem. Phys. **129**, 144107 (2008).
[82]O. Schenk and K. Gärtner, Fut. Gen. Comput. Syst. **20**, 475 (2004).